Introducing Advanced Freeform Optic Design to Li-Fi Technology

René Kirrbach[1,2], Benjamin Jakob[1,2] and Alexander Noack[1]
[1]*Fraunhofer IPMS, Maria-Reiche-Straße 2, Dresden, Germany*
[2]*Department of Electrical and Computer Engineering, TU Dresden, Dresden, Germany*

Keywords: Composite Ray Mapping, Freeform Optics, Fresnel Lenses, Li-Fi, Optical Wireless Communications, TIR Optic.

Abstract: The paper considers the potential of freeform optics for Li-Fi technology and presents design approaches for transmitter and receiver optics using ray mapping methodology and freeform Fresnel lens, respectively. Simulation results are then presented for models validation.

1 INTRODUCTION

The proceeding digitalization of our environment leads to continuously increasing mobile data traffic. The capacity provided by current radio frequency (RF) based wireless technologies such as Wi-Fi, Bluetooth will not be sufficient in the future, due to their limited frequency bands. Inter-channel interference is an emerging issue that degenerates data rate and latency of wireless links in crowded areas. The so-called "spectrum crunch" can be faced by introducing new technologies with different carrier frequencies. Besides intensive research in the field of millimeter-wave based communications (Rappaport et al., 2013), Li-Fi technology becomes more and more popular. Li-Fi utilizes visible or invisible optical wireless communication links that offer high-speed and low latency data transfer trough spatially well-defined communication channels. This allows to design cellular networks and to reduce inter-channel interference.

In the past decade different aspects of the Li-Fi technology emerged rapidly. Various modulation schemes were investigated (Islim et al., 2016), new emitters were developed (Ferreira et al., 2016) and integration of Li-Fi into existing networks was studied (Wu et al., 2017). However, despite investigation concerning fluorescence concentrators (Collins et al., 2014), modern optic design methodology for Li-Fi was not in focus of the scientific discourse. Typically, simple lenses are used for beam shaping and optical amplification. But these cannot fully serve current trends like an ongoing miniaturization of Li-Fi transceivers in order to allow their integration into other devices. Scaling down the optics is directly connected to performance degeneration. This is due to the extended source problem at transmitter side and reduced receiver gain. Advanced freeform optics can compensate the performance degeneration and provide compact, high-performance solutions precisely tailored to the application. For example, providing Li-Fi connectivity within a corridor can effectively be realized by shaping rectangular spots.

This paper demonstrates the potential of freeform optics for Li-Fi technology and gives an overview over suitable optical design methods. The rest of the paper is organized as follows: in chapter two fundamental requirements for Li-Fi optic modules are defined and limitations of standard lenses are shown. Chapter three provides an overview over different optical design concepts. In chapter four we present design examples of freeform transmitter and receiver optics and characterize them with optical simulations. Finally, chapter five gives a short summary.

2 FUNDAMENTALS

As Figure 1 illustrates, a Li-Fi module consists of a transmitter (Tx) and a receiver (Rx). The transmitter uses light emitting diodes (LEDs) or laser diodes (LDs) for signal transmission, whereas the receiver incorporates a photodiode (PD) for signal detection.

Both parts are characterized by their field-of-view (FOV). Typically, both FOVs are designed equally. However, in certain application scenarios they may differ. If Li-Fi connectivity is provided within a corridor, the fixed transmitter at the ceiling shapes a

Kirrbach, R., Jakob, B. and Noack, A.
Introducing Advanced Freeform Optic Design to Li-Fi Technology.
DOI: 10.5220/0007471802480254
In *Proceedings of the 7th International Conference on Photonics, Optics and Laser Technology (PHOTOPTICS 2019)*, pages 248-254
ISBN: 978-989-758-364-3
Copyright © 2019 by SCITEPRESS – Science and Technology Publications, Lda. All rights reserved

rectangular spot. The receiver of the mobile device below has a rotationally symmetric FOV due to the unknown orientation of both devices to each other.

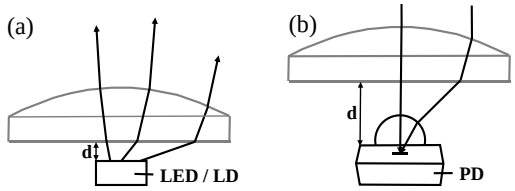

Figure 1: Li-Fi transceiver consisting of a transmitter (a) and a receiver (b). Simple systems incorporate spherical lenses as shown here.

The optical link is further characterized by its dynamic range which defines the spatial distance where data transmission is possible. It is limited by a minimum and a maximum range. Below the minimum distance the signal is too strong and the receiver runs into saturation. Above the maximum distance the signal level is below the sensitivity of the receiver. The receiver amplifier can use automatic gain control to improve the dynamic range. However, this approach has its limits. For a maximization of the dynamic range the transmitter and receiver must exhibit a homogenous behavior over their FOV. This can easily be understood if we assume for instance a strong peak in the transmitter's emission profile. The peak raises the minimum communication distance and consequently lowers the dynamic range.

2.1 Transmitter Optics Requirements

As already mentioned, LEDs or LDs are used as emitters. LDs exhibit small emission angles. Sometimes even standard aspheric lenses allow sufficient beam shaping. LEDs are isotropic emitters. Thus, efficient optic design for LEDs is more sophisticated. Fortunately, Li-Fi technology can profit from advances in freeform illumination design where LEDs are omnipresent nowadays. In contrast to illumination design, efficiency and homogeneity is even more crucial since it refers directly to range, data rate and bit error rate. Moreover, the transmitter's optical output power might be limited due to bandwidth requirements or because of the limited power budget of mobile devices.

The communication spot can be defined as the area, where the irradiance E is larger than the minimum irradiance E_{min} required for communication. The transmitter's efficiency η_{Tx} is the power that reaches the FOV divided by the total emitted power. However, η_{Tx} does not pay attention to the power distribution within the FOV. If the transceiver has a bit-loading mechanism, it adjusts its data rate to receiver's current signal level.

Yet, low-latency transceivers typically have simple modulation schemes with fixed data rate. They require a defined minimum receiver signal level and thus a minimum irradiance E_{min} in order to fulfil the specification, i.e. ensuring a bit error rate. An irradiance peak within the FOV gives no benefit, since the specification is already fulfilled with E_{min}. In fact such a peak actually reduces the dynamic range by increasing the minimum communication distance as mentioned before. Therefore, it is better to equally distribute the power within the FOV to raise E_{min} in order to maximize the range of the link. Hence, for transceivers with fixed data rate we define a more powerful figure of merit by combining efficiency and uniformity: equation (1) defines the effective transmitter efficiency $\eta_{\mathrm{Tx\,eff}}$ as the ratio of the minimum irradiance E_{min} within the FOV at the maximum distance produced by the optic to $E_{\mathrm{min\,ideal}}$. This $E_{\mathrm{min\,ideal}}$ is the irradiance achieved by an ideal optic, which concentrates 100 % of the emitted power P_{Tx} homogenously into the FOV and forms a so-called tophat profile. It is calculated by dividing the emitted power P_{Tx} by the illuminated area A_t.

$$\eta_{\mathrm{Tx\,eff}} = \frac{E_{\mathrm{min}}}{E_{\mathrm{min\,ideal}}} = \frac{E_{\mathrm{min}} A_{\mathrm{t}}}{P_{\mathrm{Tx}}} \quad (1)$$

Figure 2 illustrates a numerical example, where the FOV should have a half-angle of 17°. The LED *SFH4451* (Osram Opto Semiconductors, 2016) has an angle of half intensity of 17° and thus seems to be well suited. However, only about 30.7 % of the emitted power P_{Tx} is within the FOV and the effective transmitter efficiency is only $\eta_{\mathrm{Tx\,eff}} = 0.168$. In contrast, an ideal optic with $\eta_{\mathrm{Tx\,eff}} = 1$ reaches an minimum irradiance E_{min} which is 5.94 times (7.7 dB) higher. This corresponds to an increase of the communication range by a factor of 2.4 if the data rate is fixed. Simple transmitters use spherical lenses in order to improve the performance, as shown in Figure 1a. Table 1 summarizes the measures of all three emission profiles. Using the lens *LA1805.1* (Thorlabs, 2018) nearly doubles the efficiency to $\eta_{\mathrm{Tx}} = 0.595$. It can be seen, that the irradiance profile is still very inhomogeneous, leading to bad dynamic range and an effective efficiency of only $\eta_{\mathrm{Tx\,eff}} = 0.282$. Aspheric lenses could improve the performance, but there are still two problems: First, not all of the emitted power reaches the lens. Second, if standard lenses are used the design freedom is low and it is hard or even impossible to find an aspheric lens that ideally fits.

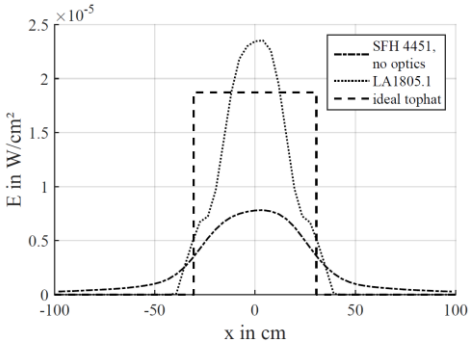

Figure 2: Irradiance along x-axis in 1 m distance for *Osram SFH4451* LED without an additional lens and with the spherical lens *LA1805.1*. The distance *d* between lens and PD is 9.6 mm (Figure 1a) and the optical power P_{Tx} is 55 mW. The tophat represents the ideal irradiance profile.

Table 1: Measures of the emission profiles from Figure 2.

Transmitter	η_{Tx}	E_{min}	$\eta_{Tx\ eff}$
SFH 4451, no optics	0.307	0.314×10^{-5} W/cm²	0.168
SFH 4451 + LA1805.1	0.595	0.529×10^{-5} W/cm²	0.282
Ideal tophat	1	1.873×10^{-5} W/cm²	1

2.2 Receiver Optics Requirements

The receiver optic introduces an optical gain g by concentrating the incident signal onto the PD.

It is well known that the optical gain g of classical optics is Étendue limited. In a 3D system g can be calculated by using equation (2) (Welford et al., 1989), where n_1 denotes the optic's refractive index and n_2 the refractive index of the surrounding medium, which is typically air. The optic's half acceptance angle is θ_a. θ_o describes the incident angle of the boundary rays from the optic to the PD chip. The maximum theoretical optical gain g_{max} is reached for $\theta_o = 90°$ (Welford et al., 1989). Therefore, the optic has to be in direct contact to the chip. Depending on how close the receiver's gain is to g_{max}, we can classify the performance of the optic module. Ideally, the gain should be constant over the entire FOV in order to achieve the maximum dynamic range. In practice however, the gain varies and we choose the angle within the FOV with the lowest gain g_{min} for classification. In order to reduce inter-channel inference and noise induced by ambient light the gain should drop rapidly outside the FOV.

$$g = \left(\frac{n_1 \sin\theta_o}{n_2 \sin\theta_a}\right)^2 \quad (2)$$

The design of receiver optics can profit from advances in optical design for solar concentration technology. Li-Fi systems typically need a greater FOV. Half-angles in the range of $5° \leq \theta_a \leq 60°$ enable the required mobility, at the expense of a lower gain. A lot of Fresnel lenses for solar concentration have been proposed (Shen et al., 2013; Koshel, 2013: 199) due to their small volume and low material costs. Fresnel lens grooves can be designed according to three different working principles (Wallhead et al. 2012): refracting, single total internal reflection (TIR) and double TIR. Combining these three working principles can improve the efficiency by reducing the Fresnel losses (Wallhead et al. 2012).

In solar concentration, a lot of secondary optical elements have been proposed (Koshel, 2013). If possible, these elements can be applied to Li-Fi modules. In practice however, the detector's active area may be some millimeters within the package and it may already include a secondary optical element. The photodetector is typically chosen because of properties like high modulation bandwidth, large area and high responsivity rather than its package geometry. In that case, the designer can tailor the primary optics precisely to the photodetectors geometry and make use of included optical elements.

Using a Compound Parabolic Concentrator (CPC) or one of its derivatives may be the right choice if their length and the detectors package is suitable. This is typically the case for large FOVs and flat packages, where the active chip area is directly below the package surface.

3 OPTIC DESIGN METHODS

3.1 Classification

Miñano (Miñano et al., 2013) separates optic design methods into two fundamental categories: numerical optimization and direct calculation.

Numerical optimization is a straight-forward method for designing complex optic modules. Modern optic simulation tools like *Optic Studio Zemax*, *FRED*, *LightTools*, etc. allow forming and optically simulating arbitrary shaped optics by overlapping parametric objects. Optimization algorithms like the *Levenberg-Marquardt algorithm* are used for adjusting parameters of these objects until a sufficiently good result is achieved. Due to the large amount of variables, the optimization is typically inefficient, because of many local minima in the merit function. This makes it hard to find the global minimum. Moreover, whenever

the system specifications change, the optimization process has to be carried out again.

In contrast, direct calculation algorithms follow well-defined design procedures and yield deterministic outcomes. This approach yields better results than numerical optimization methods (Koshel, 2013), especially if the systems are complex. With the tailored freeform design method, proposed by Ries and Muschaweck (Ries et al., 2001), the designer solves a set of non-linear equations to generate a freeform surface. However, more often geometrical calculations are used for surface construction. Various approaches are known, e.g. composite ray mapping (Ma, 2015), forming surfaces using Cartesian ovals (Michaelis et al., 2011), simultaneous multiple surface (SMS) method in 2D (Winston et al., 2005) and 3D (Benitez et al., 2004).

The edge-ray principle is used in most of these design methods. It states, that extreme rays at the input aperture edge will form the rim of the output aperture (Welford et al., 1989). We can use this principle by designing the optic for the extreme rays and assuming that all other rays lie in-between the output apertures rim. Although this assumption is not completely true in 3D, this approach still yields good results (Welford et al., 1989).

Direct calculation methods lead to deterministic results, but optimization of certain input parameters can still be a useful tool for compensating unrealistic assumptions during the calculation, like assuming a point source. In contrast to numerical optimization, less but much more effective variables are chosen. Therefore, the optimization process converges faster.

Most of the direct methods give dedicated points of the optical surfaces. Non-uniform rational B-splines (NURBS) are a powerful tool for surface interpolation. Piegl and Tiller (Piegl et al., 1995) give a detailed description on how to set up the required algorithms. NURBS are supported in the most popular CAD formats such as STEP or IGES. This is beneficial, since the calculated optic geometry has to be exported into a CAD format for optical simulation and fabrication.

3.2 Composite Ray Mapping

Composite ray mapping combines an energy mapping approach with a subsequent geometrical calculation of the optics shape by assuming a point source. An optimization step addresses the extended source problem and other unrealistic assumptions by modifying the source or target energy map or both in parallel. The method is used in this work because it is versatile, easy to understand and it has the potential to yield very efficient results.

3.2.1 Energy Mapping

Energy mapping allows the designer to transfer the emission profile of the source into a desired illumination pattern. We assume a homogenous illuminated target surface for the following considerations. Typically, the half-space around the source is divided into areas in such a way that the same amount of energy is emitted trough each surface element. Next, the target surface is divided into parts of equal size. Each surface element of the source map is linked to a corresponding element of the target map. If the optic module is able to provide this link, a homogenous illuminated spot is formed.

The coordinate system that is used for creation of the energy maps strongly influences the optics performance. This is because of a surface error that appears during the geometrical calculation of the optic surfaces (Ma, 2015; Wang et al., 2017). The coordinate system determines the magnitude of this surface error. For circular spots, we recommend a spherical coordinate system for the source map and a radial energy map for the target as Wang et al. described (Wang et al., 2017). For rectangular spots the author recommends a double-pole coordinate system for the source as Ma proposed (Ma, 2015).

3.2.2 Geometrical Calculation

The edge points of the surface elements of the source and target energy map are used as unit vectors for the input and the output rays. An initial surface point for calculation has to be defined. The following point is calculated by using the surface normal of the previous point and the next input ray. Thereby an initial curve of the surface is calculated. For rotationally symmetric optics, that curve is rotated around the optical axis. For non-rotationally symmetric optics, multiple curves are calculated. Typically, a quarter or half of the geometry is calculated and the rest is generated by mirroring. Detailed information concerning the calculation algorithm and about the composite ray mapping methodology in general can be found in the work of Ma (Ma, 2015) and Wang (Wang et al., 2017).

3.2.3 Optimization

During the calculation some false assumptions were made which lead to a surface error that can be corrected by optimization. These false assumptions may include: the point source model, a mismatch between the source and target energy map (Ma, 2015) and monochromatic light. A purposeful distortion of the source energy map, the target energy map or both simultaneously can address these false assumptions. Therefore, the

designer should parametrize the energy maps with a minimum number of parameters to enable an effective optimization.

4 DESIGN EXAMPLES

All simulations are based on optical ray tracing using *Optic Studio Zemax 17*. The simulations incorporate realistic simulation models like the corresponding ray files and spectrum files. No anti-reflection (AR) coatings are used. For the emitter, the infra-red LED *Osram SFH4451* (Osram Opto Semiconductors, 2016) is used with 55 mW optical power. The receiver incorporates a *Hamamatsu S10784* (Hamamatsu, 2013) PD. The PD package includes a spherically shaped lens.

4.1 Transmitter Optics

4.1.1 Design

LED chips are isotropic emitters. In order to maximize the transmitters efficiency the optic has to surround the emitter. Illumination systems typically incorporate a reflector. This approach can provide a homogenous power distribution at the center of the FOV. But its efficiency is limited due to absorption losses (Koshel, R. J., 2013) and the reflectors tend to be large. For small reflectors on the other hand, the steepness at the edge of the FOV is poor as we can see in Chaves example designs (Chaves, J., 2016). The reflector approach is still an interesting low cost solution: transmitter and receiver can have separated reflectors, but both can be placed on the same carrier and fabricated simultaneously. The reflector can be calculated by traditional methods (Chaves, 2016) or by using the composite ray mapping methodology. The latter can face the extended source issue and can easily be applied to any kind of source profile.

For high-performance designs, there are two different design approaches. Figure 3 shows a design based only on refraction, whereas the design from Figure 4 has at least one interface with TIR. Both optics were realized using composite ray mapping methodology with a spherical coordinate system for the source map and a radial energy map for the target plane. The design in Figure 3 is suitable for large FOV. This is due to the limited deflection of two refractions and increasing Fresnel losses with large refraction angles. Moreover, it tends to be thick for relatively small FOVs. The design in Figure 4 is more complex and should be used for small and medium FOV. For a rectangular spot, non-rotationally symmetric versions of both designs can be derived.

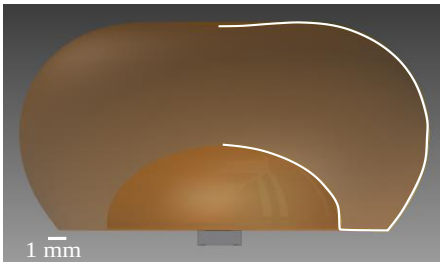

Figure 3: Transmitter optic based on refraction. The body is formed by rotating the white spline around the optical axis. It is 22 mm in diameter, 12 mm in height and forms a FOV with a half-angle of 37°.

Figure 4: Transmitter optic based on refraction and TIR. The body is formed by rotating the white spline around the optical axis. It forms a FOV with half-angle of 17°. The optics diameter is 25 mm and its height is 10 mm.

4.1.2 Results and Discussion

The following considerations stick to the anticipated FOV with half-angle of 17°. Therefore, only the TIR optic in Figure 4 is considered. Figure 5 shows the irradiance at 1 m distance. We get $\eta_{\mathrm{Tx}} = 0.74$ and $E_{\mathrm{min}} = 1.25 \times 10^{-5}$ W/cm² which results in $\eta_{\mathrm{Tx\,eff}} = 0.69$. In comparison to the *SFH4451* LED without additional optics this is an improvement by a factor of 3.98 (5.99 dB). Even compared to the spherical lens *LA1805.1* from Figure 2 E_{min} is increased 2.36 times (3.73 dB).

The simulation shows, that 10.5 % of the emitted power is lost due to Fresnel reflections. This could be reduced by depositing an AR coating. However, the shape of the optic makes it difficult to deposit homogenous layers. Another 15.5 % of the power misses the FOV due to the extended source problem. By scaling up the optic this loss can be reduced.
Moreover, 5% of the "losses" for $\eta_{\mathrm{Tx\,eff}}$ result from inhomogeneity. The white circle in Figure 5 marks the minimum within the FOV. The ray file of the *SFH4451* reveals that this minimum is not caused by the optic, but by the reflector within the LED package, which is not fully rotational symmetric.

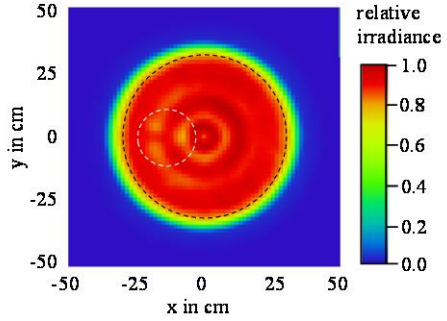

Figure 5: Irradiance in 1 m distance. The black circle marks the FOV. The white circle highlights minimum.

4.2 Receiver Optics

4.2.1 Design

The Fresnel lens shown in Figure 6 is precisely tailored to the PD and provides a FOV with a half-angle $\theta_a = 17°$. It is 2.5 mm thick and has a refracting section in the center surrounded by one TIR groove. The thickness could be further reduced if both sections are divided into multiple grooves. For the initial design the edge-ray principle was applied for all surfaces. Due to the discontinuity between both sections, the edge-ray principle is not valid for the complete input aperture. Therefore, the gain is not constant within the FOV. A homogenization can be achieved by slightly adjusting the groove for a range of incident angles rather than only for the maximum incident angle. The designer has to be aware of shading effects within the grooves for rays with large incident angles. Due to non-ideal rays the actual performance at the edge of the FOV will be worse than one may expect in the first place. These rays emerge for example from polychromatic light or they are simply skew rays. The issue can be addressed by directing the rays not directly the edge of the PD active area but slightly next to this edge.

For comparison, a second receiver with the spherical lens *LA1074.1* (Thorlabs, 2018) is designed, as depicted in Figure 1b. The lens has a diameter of 12.7 mm and the distance *d* to the PD is 2 mm.

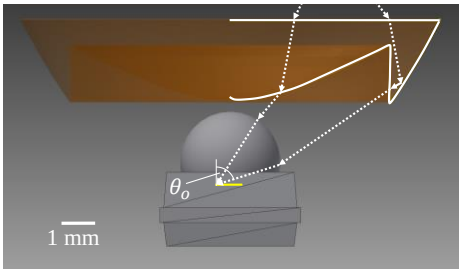

Figure 6: Freeform Fresnel lens tailored to PD *S10784*. The lens is 12.5 mm in diameter and 2.5 mm in height. The cross sectional spline is colored white and the active area yellow.

4.2.2 Results and Discussion

Figure 7 shows the gain over the angle of incidence θ_i. The gain of the Fresnel lens is 15.5. This is 1.8 times (2.6 dB) higher than the gain of the spherical lens, which is 8.5. Moreover, the gain of the Fresnel lens drops much faster the outside FOV. This effectively reduces inter-channel interference and shot noise induced by ambient light. According to Figure 7, 15 % of the power is lost due to Fresnel reflections. These losses can be reduced by applying an AR coating at least at the flat top surface of the lens. Despite the Fresnel losses, the minimum gain g_{min} is still about 25 % below the ideal gain g_{max}. Three reasons for that can be derived from the design procedure. First, the freeform lens directs the rays onto the spherical lens. The maximum coupling angle θ_o to the active chip is only 73.5° instead of the ideal 90°. Second, the rays are not directed directly on to the chip edge, but slightly next to it. Therefore, the calculated lens is smaller and thus its gain is lower than g_{max}. Third, due to the discontinuity, the edge-ray principle is not fully satisfied and losses occur.

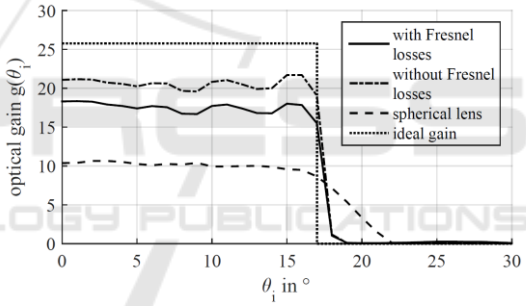

Figure 7: Optical gain *g* of the Fresnel lens and the spherical lens *LA1074.1* in conjunction with PD *S10784* over angle of incidence θ_i. The ideal gain was calculated with equation 2 assuming $n_1 = 1.49$, $n_2 = 1$, $\theta_a = 17°$ and $\theta_o = 90°$.

4.3 Complete Optical Channel

Figure 8 shows the incident optical power onto the PD active area $P_{pd\,opt}$ over the FOV for transceivers without optics, with spherical lenses and with the freeform lenses from section 4. The freeform lenses provide a homogenous signal level within the FOV. It varies only about 1.3 dB and never drops below -24.1 dBm. In contrast, the signal level provided by the spherical lenses fluctuates by 7.5 dB and drops at the edge to -30 dBm. This inhomogeneity is caused by the spherical transmitter lens. The simulation without any optics show signal levels down to -36.1dBm. This simulation is noisy, because only a small amount of rays hit the detector and the initial number of rays is limited by the

ray file.

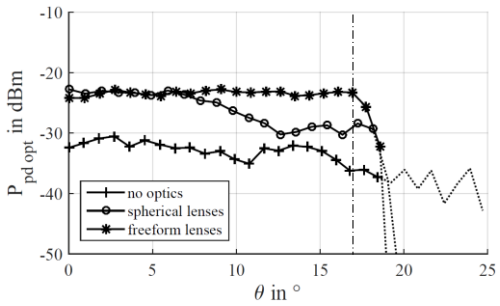

Figure 8: Incident optical power $P_{pd\ opt}$ onto the PD active area over FOV for no optics, spherical lenses (*LA1805.1*, *LA1074.1*) and freeform lenses. The angle θ corresponds to a misalignment of both transceivers in the plane over a distance of 50 cm. The graphs are very noisy in the dotted region, because only a few rays hit the PD surface.

5 CONCLUSIONS

This paper demonstrates the potential of modern freeform optics for Li-Fi technology. Design strategies for transmitter optics are discussed and a TIR based optic is presented and characterized. The design example proofs that composite ray mapping is an efficient tool for shaping homogenous emission profiles. For the receiver, the designer should tailor the optic precisely to the PD. A Fresnel lens based on refraction and TIR is proposed and it is shown that the optical gain is about 2.6 dB higher compared to a conventional spherical lens for the considered PD.

We show that the proposed freeform optics provide a minimum signal level which is 5.9 dB higher than a optic setup with spherical lenses. The signal level has an excellent homogeneity within the FOV and fluctuates only by 1.3 dB. This is about 6.2 dB less compared to the proposed spherical lenses. This high homogeneity maximizes the dynamic range and the sharp cut-off at the edge of the FOV effectively reduces inter-channel interference and noise.

Our next steps will include the fabrication and experimental characterization of the designs. Finally, transmitter and receiver optics should be combined to one hybrid optic module for size and cost reduction.

REFERENCES

Barry, J. R., 1994. Wireless Infrared Communications. In *The Springer International Series in Engineering and Computer Science*, 1st ed., Springer US, 181, 265-289.

Benitez, P. G., Miñano, J.C., et al., July 1, 2004, Simultaneous multiple surface optical design method in three dimensions. In *Optical Engineering*, vol. 43, no. 7, 1489–1502.

Caves, J., 2016. Introduction to Nonimaging Optics. 2nd Edition, *CRC Press*, 259-319.

Collins, St., O'Brien, D. C., Watt, A., 2014. High gain, wide field of view concentrators for optical communications. In *Optics Letters* vol. 39, no. 7, 1756-1759.

Dross, O. et al., 2004, Review of SMS Design Methods and Real World Applications. In *Proceedings of SPIE 5529 - The International Society for Optical Engineering*.

Ferreira, R. X. G. et al. Oct 1, 2016, High Bandwidth GaN-Based Micro-LEDs for Multi-Gb/s Visible Light Communications. In *IEEE Photonics Technology Letters*, vol. 28, no. 19, 2023-2026.

Hamamatsu Photonics, May 2013. S 10784. Datasheet.

Islim, M. S., Haas, H., 2016. Modulation Techniques for Li-Fi. In *ZTE Communications*, vol. 14, no. 2, 29-40.

Koshel, R. J., 2013. Illumination Engineering: Design of Nonimaging Optics. Wiley-IEEE Press, 17,190,199.

Ma, D., 2015. Exploration of Ray Mapping Methodology in Freeform Optics, The University of Arizona, 38, 61, 66-95.

Michaelis, D., et al. 2011. Cartesian oval representation of freeform optics in illumination systems, in *Optical Letters*, 36(6), Optical Society of America, 918-920.

Miñano, J.C. et al, 2013. SMS 3D Design Method, Chapter 4 in *Illumination Engineering: Design of Nonimaging Optics*. Wiley-IEEE Press, 102.

Osram Opto Semiconductors, 26.06.2016. SFH 4451. Datasheet, ver. 1.6.

Piegl, L., Tiller, W., J., 1995. *The NURBS Book*, Springer. Berlin-Heidelberg, 2nd Edition.

Rappaport, T. S. et al. May 10, 2013. Millimeter Wave Mobile Communications for 5G Cellular: It Will Work!. In *IEEE Access*, 1 (2013), 335-349.

Ries, H., Muschaweck, J., April, 2002, Tailored freeform optical surfaces. In *Journal of the Optical Society of America A*, 19(3):590-5, Optical Society of America.

Shen, S. C., et al., 2013. A Novel TIR-R Concentration Module of Uniformly Solar Energy for HCPV Systems. *In Proceedings of the 2013 IEEE/SICE International Symposium on System Integration*, Kobe, 747-752.

Thorlabs, LA1074,[online]www.thorlabs.com, 12.11.2018.

Thorlabs, LA1805,[online]www.thorlabs.com, 12.11.2018.

Wallhead, I., et al. 2012. Design of an efficient Fresnel-type lens utilizing double total internal reflection for solar energy collection, in *Optics Express*, vol. 20, no. S6, Optical Society of America.

Wang, K., Liu, S., Xiaobing, L. Wu, D., September 2017. Freeform Optics for LED Packages and Applications, *Wiley*, 1st Edition, 25, 53-54, 58-60.

Welford, W. T., Winston, R., 1989. High Collection Nonimaging Optics, *Academic Press Inc.*, San Diego, 1st Edition, 21-22, 54.

Winston, R., Miñano, J.C., Benitez, P. G., 2015. Non-imaging Optics. *Elsevier Academic Press*,181-217.

Wu, X. , Safari, M., Haas, H., 2017. Access Point Selection for Hybrid Li-Fi and Wi-Fi Networks, in *IEEE , Transactions on Communications, vol. 65, no. 12, 5375-5383*